IIII Original Paper IIII

Long-term Behaviors of a Single Particle Forming a Coherent Structure in Thermocapillary-driven Convection in Half-zone Liquid Bridge of High Prandtl-number Fluid

Kengo YAMAGUCHI [1], Takuma HORI [2, 3] and Ichiro UENO [2, 3]

Abstract

We experimentally investigate behaviors of a single spherical particle in a half-zone liquid bridge induced by the thermocapillary effect. It has been indicated that suspended particles show unique structures in time-dependent traveling flow state. This phenomenon is called 'particle accumulation structure (PAS).' In order to understand correlation between the identical particle motion and the coherent structures by the particles, we focus on a single particle behavior to illustrate the spatio-temporal correlation between PAS itself and individual particles on PAS. We indicate the Poincaré section for the particle forming PAS and that forming the toroidal core by preparing a thin light sheet. Through a long-period observation of the turnover motion of individual particle, we make comparison with the proposed topological flow fields accompanying with so-called Kolmogorov-Arnold-Moser (KAM) tori. The present work is conducted as a ground-based research for coming on-orbit international collaborative experiments aboard the Japanese Experiment Module 'Kibo' in the International Space Station by the project of Japanese-European Research Experiment on Marangoni Instability (JEREMI).

Keyword(s): Thermocapillary-driven convection, Coherent structure, Particle accumulation structure, Half-zone liquid bridge, Poincaré section
Received 22 January 2019; Accepted 8 April 2019; Published 30 April 2019

1. Introduction

1.1 Space Experiments on Marangoni Convection on the ISS

Series of fluid physics experiments on thermocapillary-driven convection in the liquid-bridge geometry had been conducted in the Japanese Experiment Module 'Kibo' aboard the International Space Station (ISS) by use of the Fluid Physics Experiment Facility (FPEF) [1]. The first project known as 'MEIS', Marangoni Experiments in Space, had brought the knowledge on the condition of the primary instability due to so-called hydrothermal wave (HTW) instability [2,3] and convective fields under microgravity conditions in the liquid bridge of a range of high Prandtl number fluids and various shapes [4–8]. This project also accumulated the knowledge on transition process of the convective field toward chaotic and turbulent regemes [9,10], and particle accumulation structures in hanging droplet geometry [11]. These were the very first series of experiments conducted on the 'Kibo.' Then another series of experiments followed MEIS. This project, so-called 'Dynamic Surf,' had been conducted focusing on the dynamic surface deformation due to the convective flow fields, and on the effect of heat transfer through the free surface on the flow transitions [12–14].

Based on these knowledges accumulated through the series of the microgravity experiments on the 'Kibo,' it has been found that the primary instability due to HTW is more sensitive to the heat transfer through the interface than discussed with simplified model by use of Biot number Bi as a control parameter. At the same time, unique behaviors of the suspended particles in the liquids have been attracted the researchers after Schwabe et al. [15]. An international collaboration among Japanese and European research groups has been organized to investigate those two major topics, and prepared the future experiments in the 'Kibo' as a project so-called 'JEREMI,' Japanese-European Research Experiment on Marangoni Instability [16,17].

The present work is conducted as a ground-based research for coming on-orbit international collaborative experiments focusing on the unique behaviors of the suspended particles.

1.2 Thermocapillrry-driven Convection in Liquid-bridge Geometries

Surface tension, γ, varies against temperature T and/or concentration C in case the coefficients of surface tension for those are not zero. It is generally known that the sign of the temperature/concentration coefficient of surface tension is negative; the fluid over the free surface is driven toward the region with lower temperature/concentration. Such phenomenon is so-called 'Marangoni effect.' Marangoni effect results in a convection in

---

1 Div. Mechanical Engineering, School of Science & Technology, Tokyo University of Science, 2641 Yamazaki, Noda, Chiba 278-8510, Japan.
2 Dept. Mechanical Engineering, Faculty of Science & Technology, Tokyo University of Science, 2641 Yamazaki, Noda, Chiba 278-8510, Japan.
3 Research Institute for Science & Technology, Tokyo University of Science, 2641 Yamazaki, Noda, Chiba 278-8510, Japan.
  (E-mail: ich@rs.tus.ac.jp)

the bulk due to the viscosity. Especially in the case due to the temperature dependence of the surface tension, such convection is called 'thermocapillary-driven' convection.

The thermocapillary flow has been studied in various systems, such as, a half zone (HZ) liquid bridge, where a designated amount of liquid is 'bridged' between two cylindrical coaxial rods. In this system, thermocapillary flow is generated by imposing a designated temperature difference between both ends of the rods. The intensity of the thermocapillary-driven convection is described with a non-dimensional Marangoni number Ma as follows;

$$\text{Ma} = \frac{|\gamma_T|\Delta T H}{\rho \nu \kappa}, \tag{1}$$

where $\gamma_T = \partial \gamma / \partial T$ is the temperature coefficient of the surface tension γ of the fluid, $\Delta T (= T_{\text{h}} - T_{\text{c}})$ the temperature difference between the top rod at T_{h} and bottom rod at T_{c}, H the height of liquid bridge, ρ, ν and κ are the density, the kinematic viscosity, and the thermal diffusivity of the liquid, respectively. A steady flow is induced with small temperature difference. It has been known that the convection exhibits a transition to a three-dimensional time-dependent 'oscillatory' convection from a two-dimensional time-independent 'steady' one by increasing the temperature difference in the case of high-Prandtl-number fluid ($\text{Pr} = \nu/\kappa \gtrsim 1$)[18]. This transition is considered to be due to HTW instability[3]. Fujimura[19] indicated the threshold between the low and high Pr to be $\text{Pr} = 0.0578$ in the liquid bridge of unity in aspect ratio $\Gamma = H/R$, where R is the radius of the disks to sustain the liquid bridge (note that Fujimura[19] defined the aspect ratio as R/H instead). After the transition due to the primary instability, it has been known that there exist two different types of oscillatory convections: the standing-wave-type oscillation and the traveling-wave-type oscillation depending on the shape of the liquid bridge and/or the thermal boundary conditions on the liquid bridge[10,20–22]. In such oscillatory convections, thermal wave appears with a standing- or a traveling-wave-type behavior on the free surface accompanying with the flow field induced by HTW. If one further increases ΔT or Ma, chaotic flow emerges[10,20,22].

1.3 Particle Accumulation Structures (PAS)

Under certain limited conditions in the regime of the traveling-wave-type convection before the chaotic state emerges, Schwabe et al.[15] found that suspended tiny particles gather to form a three-dimensional closed coherent structure, so-called 'particle accumulation structure (PAS).' It has been indicated that such unique structures emerge even with tiny particles of high tracer fidelity to the fluid motion in terms of Stokes number St. This structure seems to rotate accompanying with HTW as an apparent rigid structure[23,24]. After the pioneering work by Schwabe et al.[15] various studies have been conducted on PAS. Tanaka et al.[23] experimentally revealed the occurrence condition of PAS against ΔT and Γ. They also classified two types of PAS in terms of

the winding number of the structure near the free surface; spiral-loop 1 (SL1) and spiral-loop 2 (SL2) PASs, and reconstructed their three-dimensional structures qualitatively based on the observations from the top as well as from the side. Their three-dimensional structures were investigated more in detail by applying particle tracking method[25,26]. It is noted that they illustrated the temporal variation of the positions of a single particle on PAS for rather short up to several periods of the turnover motions of the particle, because of the limitation of the data storage for the high-speed observations. Thus the durability for the particle forming PAS has never been discussed.

In addition to the discussion on occurring conditions and the spatial correlation between PAS and the particles, physical mechanism has been also discussed; how the particles are attracted to form coherent structures inside the liquid bridge. Schwabe et al.[24] proposed a mechanism of the formation of PAS based on the observation by the experiment by considering the correlation between the temperature distribution over the free surface and the position of PAS inside the liquid bridge. They considered that the particles gathered near the free surface before traveling back inward the liquid bridge due to the non-uniform temperature distribution by HTW. It was found, however, that this spatial correlation is not universal against the variation of Pr[27]. After the proposal of the mechanism by Schwabe et al.[24], investigations via theoretical and numerical approaches have been conducted to explain how the particles gather. There exist two major physical models to explain the accumulation of the particle inside the liquid bridge; phase-locking model[28] and particle-surface interaction model[29]. The former proposed that the synchronization between the inertia-dominant motions of the particles and HTW was essential. The latter proposed that the interaction between the particles with a finite size and the free surface was essential process for the particles to change the streamline to follow, which resulted in the accumulation along a certain line. Discussion had been made by monitoring formation time of PAS[24] as well as predicted shape of PAS, and it was concluded that the interaction between the particles and the free surface would explain better the physical process of the PAS formation[30]. The physical model based on the particle-surface interaction was also validated especially focusing on the behavior of a single particle in two-dimensional convection[31].

Those studies have brought knowledges that indicate 'how' the particles accumulate within the thermocapillary liquid bridge. There exist another series of discussion 'where' the particles accumulate inside the liquid bridge, or, 'where' in the convection field attract the particles. Kuhlmann & Muldoon[32] and Mukin & Kuhlmann[33] illustrated the existence of closed stream tubes in the rotating frame of reference, called Kolmogorov-Arnold-Moser (KAM) tori, as well as chaotic region in the liquid bridge by employing a traveling-wave-type model convection of high-Prandtl-number fluid (Pr = 4). The KAM tori are stationary rigid

under a certain condition in terms of $Re = Ma/Pr$ in the rotating frame of reference, that is, the structures exhibit a rigid-body-like rotating motion with the same azimuthal velocity in the absolute coordinate system as PAS. The flow fields consisting of KAM are thus realized below the threshold for the secondary instability in which the flow in the rotating frame of reference against the fundamental frequency of HTW becomes time-dependent[34]. It was then indicated through the experiment as well that the PAS, the toroidal core[23], and additional structure wrapping the core observed in the liquid bridge emerge simultaneously as predicted with the model flow field[35]. Romanò & Kuhlmann[36] conducted a series of direct numerical simulation with the PSI model for $Pr = 28$ liquid bridge, and successfully reproduced the particle accumulation in such a high-Prandtl-number fluid. They showed the Poincaré section of the particles on PAS's to make comparison with the KAM tori predicted, and also indicated that the toroidal core becomes weakly chaotic in such a high Pr fluid.

In this research, the objective is to detect the Poincaré section to reflect the distribution of the particles on PAS in the liquid bridge experimentally, and investigate the interaction between the particle and KAM tori. We especially focus on the long-term behavior of a single spherical particle to indicate correlation among PAS itself, the individual particle to form PAS, and KAM tori.

2. Experiment

Figure 1 illustrates the schematics of the experimental appa-ratus. The apparatus is basically the same as the previous stud-ies[27,37].

A designated amount of the liquid is sustained between two rods facing each other concentrically. The top rod is made of sapphire. The radius of the end surfaces to sustain the liquid R is of 2.5 mm. A heater of a nichrome wire is wound around the top rod. Temperature of the top rod is measured by K-type thermocouple embedded in the top rod. The thermocouple and the heater are connected to the temperature controller (Model 335 Cryogenic Temperature Controller, Lake Shore Cryotron-ics Inc., USA), and the temperature of the rod is adjusted by

Fig. 1 Experimental apparatus

PID (proportional-integral-derivative) control. The bottom rod is made of aluminum rod of 2.5 mm in radius at the end. In order to prevent liquid dripping from the bottom rod, its upper edge is tapered at 45°, and is coated with fluorine. A small hole is drilled through along the center of bottom rod, and the test fluid is supplied through that hole connected to the syringe pump with a tube. The temperature at the bottom rod is kept at 20 °C by using a cooling channel through a base block of the bottom rod. We fix, through this study, the aspect ratio of the liquid bridge $\Gamma = H/R$ at 0.68, where H is the distance between the end surfaces to sustain the liquid, or the height of the liquid bridge.

A glass shield of 25 mm in inner diameter and of 1.5 mm in thickness encloses the liquid bridge concentrically. This external shield enables us to fix the thermal boundary conditions around the liquid bridge by suppressing undesignated flows in the ambi-ent gas region. A germanium window is installed at a tiny part in azimuthal direction of the shield, which allows us to monitor the surface temperature via an infrared (IR) camera (Thermography R300, NEC Avio Infrared Technologies Co., Ltd., Japan) with a closeup lens (TVC-2100UB, NEC Avio Infrared Technologies Co., Ltd., Japan). We record the signal via the IR camera at a fixed frame rate of 60 fps with a temperature resolution of 0.05 K at 30 °C. The sensor of this IR camera detects the infrared light in a range of 8 μm to 14 μm in wavelength. We also monitor the shape of the liquid bridge through the shield in order to confirm the volume ratio of the liquid bridge, V/V_0, where V is the total volume of the liquid bridge itself, and V_0 is the volume between the end surfaces corresponding to $\pi R^2 H$. The volume ratio is kept constant as $V/V_0 \sim 1 \pm 0.1$ by supplying the test liquid through the hole via the syringe pump. The test liquid is supplied at a minimum rate to keep the volume ratio in order to prevent any disturbances to the flow field by injection.

The test liquid is 2-cSt silicone oil (KF96L-2cs, Shin-Etsu Chemical Co., Ltd., Japan) of $Pr = 28.5$ at 25 °C. The density ρ [kg/m^3], kinematic viscosity ν [m^2/s], thermal diffusivity κ [m^2/s], surface tension γ [N/m] and its temperature coefficient γ_T [N/(m · K)] are of 8.7×10^2, 2.0×10^{-6}, 7.02×10^{-8}, 18.3×10^{-3} and -7×10^{-5}. One finds those properties except γ_T in the data sheet provided by the product company[38]. It has been confirmed that one can firmly realize both of SL-1 and SL-2 PAS's with the azimuthal wave number $m = 3$ with this test fluid under the con-dition concerned[27].

In the present study, tiny particles of the order to the several tens micrometer in diameter are suspended as the test particles. We prepare two different types of the particles. The one is gold-nickel-alloy coated acrylic particles for detecting the whole struc-tures of PAS and the toroidal core as conducted by Toyama et al.[27]. The diameter and density of this particle are of 30 μm and 1.49×10^3 kg/m^3, respectively. One can detect the shape of PAS, the rotating direction of HTW, and the spatio-temporal correlation between PAS and the thermal wave over the free sur-
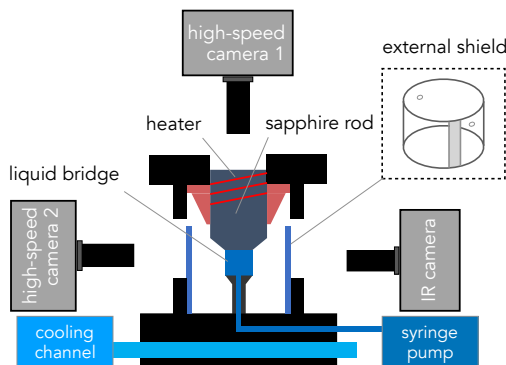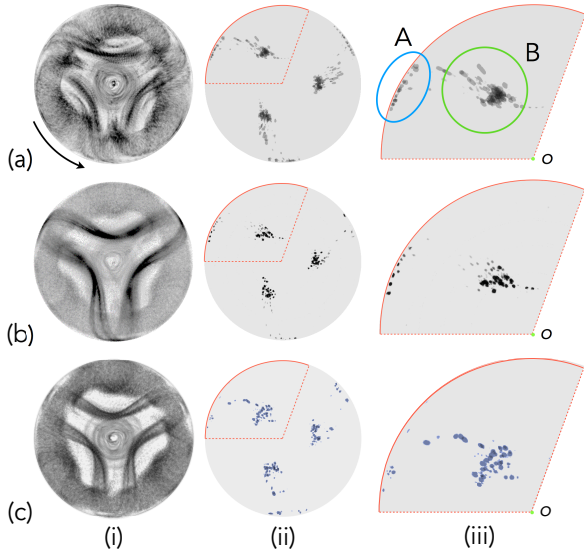
Fig. 2 PASs observed through top rod in rotating frame of reference against fundamental frequency of hydrothermal wave (HTW) under Ma = (a) 4.1×10^4, (b) 4.7×10^4, and (c) 5.2×10^4. Columns (i) and (ii) indicate the projected images, and Poincaré sections at midheight of liquid bridge, respectively. Images for column (i) are obtained by by integrating 500 frames (for about 8.3 s). Images for column (ii) (a) and (b) are obtained by integrating 3900 frames (for almost 65 s), and (c) 2340 frames (for almost 39 s). Column (iii) shows a zoomed view of $1/3 = 1/m_0$ region of image in (ii). The fundamental frequencies f_0 are of (a) 1.41 Hz, (b) 1.42 Hz, and (c) 1.44 Hz. The rotating direction of the HTW in this figure is counter-clockwise in the laboratory frame.

Fig. 3 Temporal variations of (top) r- and (bottom) θ-positions of a particle to form PAS on Poincaré section under Ma $= 4.1 \times 10^4$. Data correspond to those illustrated in Fig. 2 (a)-(ii) . Dashed line in the top frame indicates the radius of the end-surfaces of the rods to sustain the liquid bridge. Histogram on the right of top graph illustrates the particle number density measured with a constant interval $\Delta r = 0.1$ mm in the observation period.

face detected by the IR camera. The other is a fluorescent particle (ThermoScientific$^{\mathrm{TM}}$ $36 - 4$, Thermo Fisher Scientific Inc., USA). We suspend a single fluorescent particle of 31 μm in diameter and of 1.05×10^3 kg/m^3 in density in addition to the gold-nickel-alloy coated particles to derive the Poincaré section of PAS simultaneously in a single experimental run. The wavelength of the maximum emission intensity is of 612 nm, and the Stokes shift is of 70 nm. Note that the Stokes number as well as the size of those two particles are almost the same in order for the particles to form almost the same structure of PAS. The Stokes number is defined as St $= \rho d_{\mathrm{p}}^2/(18H^2)$, where ρ is the density ratio between the particle ρ_{p} and the test fluid ρ_{f}, and d_{p} the particle diameter[29]. The Stokes numbers for the gold-coated-acrylic particle and fluorescent particle are evaluated as 3.0×10^{-5} and 2.2×10^{-5}, respectively. Note that we measure the diameter of particles before each experimental run with the same process as Romanò et al.[31]. It is emphasized that PAS does not form if one put two kinds of particles of different size even though PAS would form if each type of the particles is mixed into a liquid bridge[39]. Therefore, in this experiment, we have chosen the particles of approximately identical size and Stokes number in order to minimize the negative influence on the PAS formation.
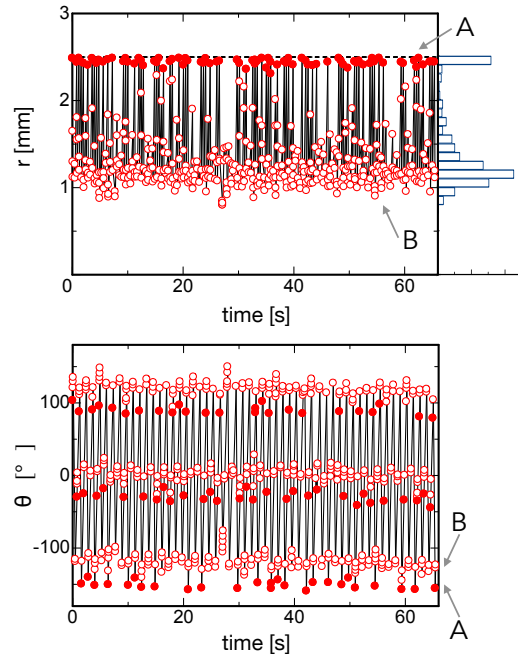
We monitors the motions of the particles through the transparent top rod with a high-speed camera (FASTCAM Mini WX100, Photron, Inc., Japan). For visualizing the whole PAS, the metal halide lamp is employed. For visualizing a single fluorescent particle, we prepare a sheet of light of 532 nm in wavelength. A sharp cut filter with a transmission limit wavelength of 560 nm is set between the camera and the top rod to capture the position of the fluorescent particle in the Poincaré section independently. One can derive the correlation between the whole PAS and a single particle on PAS by turning on and off the light sheet.

3. Results & Discussion

As indicated by previous researches[23,27], variations of PAS are realized by changing Marangoni number. Figure 2 (i) shows PASs observed through the top rod in the rotating frame of reference against the fundamental frequency of the HTW under Ma = (a) 4.1×10^4, (b) 4.7×10^4, and (c) 5.2×10^4. These conditions are realized under ΔT = (a) 36 K, (b) 40 K and (c) 44 K. The fundamental frequencies f_0 are evaluated as (a) 1.41 Hz, (b) 1.42 Hz, and (c) 1.44 Hz. The rotating direction of the HTW in each frame is counter-clockwise in the laboratory frame.

Entire views of distributions of a number of particles in the liquid bridge are illustrated in the column (i). It is noted that the

top-view images are detected through the transparent top rod by illuminating almost of all region of the liquid bridge. That means, these images correspond to the projected images of the particles, and one cannot obtain any information on the three dimensional positions of the particles. These images are obtained by superimposing 500 frames (for about 8.3 s). Under these conditions, the particles are attracted to form PAS of $m = 3$, and the toroidal core as aforementioned. The shape of this PAS is quite similar to the KAM torus of T_3^3, and that of the core to the KAM of T_{core} as indicated by Mukin & Kuhlmann[33]. Such correlation between the predicted KAM tori and experimental results was firstly illustrated by Kuhlmann et al.[35] Note that the fundamental frequencies of HTW and PAS are the same[23]. In the case with azimuthal wave number m, one obtains the same flow field in every fundamental period of $1/f_0$; the convective field rotates $2\pi/m$ during this period due to the symmetry of the flow field, supposing $2\pi/m$-symmetric structure along z axis. Thus, the period of 8.3 s for accumulating the images to obtain the projected images corresponds to almost 6 fundamental periods of HTW or $6/m = 2$ rotations of the whole structure without considering the symmetry. Even accumulating images for rather short periods, one can obtained more significant information on the coherent structures realized in the liquid bridge comparing to the instant images.

We then focus on the behaviors of a single particle forming PAS. The images in the column (ii) illustrate the Poincaré section at the midheight of the liquid bridge obtained by integrating 3900 frames (for almost 65 s) for (a) and (b), and by integrating 2340 frames (for almost 39 s) for (c). These images consist of the paths of the particles on PAS in the midplain. Note that the period of 65 s for accumulating the images to obtain the projected images corresponds to almost 45 fundamental periods of HTW. Because we track a single particle in the liquid bridge, we accumulate the images for longer periods to visualize the single particle's paths on the section. It is noted again that the image in frame (ii) is obtained in the same experimental run shown in frame (i) but in different period. There exist three sets of the pair of the dense paths as indicated in 'A' and 'B' as indicated in **Fig. 2 (a)-(iii)** ; the pair consists of a region located in the vicinity of the free surface (one of the three dense regions is indicated as 'A' in a zoomed view in frame (iii)), and another located in the middle of the liquid bridge in these Poincaré section (one of them is indicated as 'B' in (iii) as well). The Poincaré section consisting these regions of dense paths is in agreement in quality with the prediction in the model flow with $Pr = 4$[33]. The region 'A' corresponds to the intersections by the particle on PAS falling down near the hot disk toward the cold one. The region 'B', on the other hand, corresponds to those by the particle arising near the cold disk toward the hot one. We find that the dense paths in the middle come closer toward the center of the liquid bridge with changing these shape more broaden in the azimuthal direction as increasing Ma. In the vicinity of the free surface, on the other hand, the distribution of the
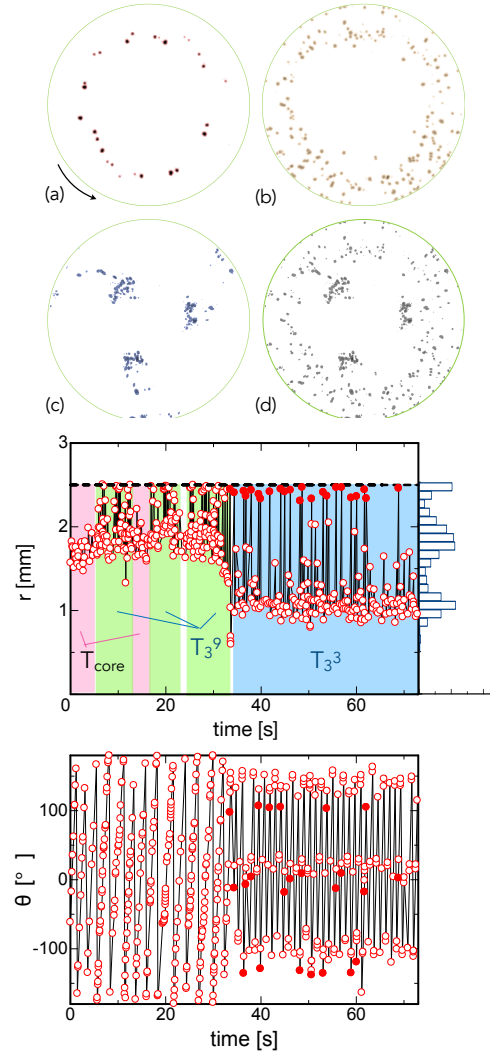

Fig. 4 (top) Poincaré section at midheight of liquid bridge obtained by integrating (a) $0 \leq t$ [s] ≤ 6.1, (b) $6.1 \leq t \leq 33.4$, (c) $33.4 \leq t \leq 73.2$ and (d) total images of the section for 73.2 s detected at z [mm] $= 0.81 \pm 0.09$ under Ma $= 5.2 \times 10^4$ (same as row (c) in Fig. 2 but in the different experimental run). (middle) and (bottom) Corresponding temporal variations of r- and θ-positions of a particle on Poincaré section. Histogram on the right of top graph illustrates the particle number density measured with a constant interval $\Delta r = 0.1$ mm in the observation period. The direction of HTW is counterclockwise in the laboratory frame in this case.

paths becomes more coarse with higher Ma.

It must be emphasized that the Poincaré section (shown in the columns (ii) and (iii)) exhibits a set of trajectories of a single particle forming PAS. It is indicated that, once the particle is attracted to form PAS under rather lower Ma (Ma $= 4.1 \times 10^4$), the particle keeps traveling along almost the same trajectory to form PAS, and it is quite seldom for the particle to change its trajectory to form the core nor a structure wrapping the core nor the rest of the region defined as 'chaotic sea.'[33] Figure 3 illustrates tempo-

ral variations of the particle concerned to illustrate the Poincaré section shown in **Fig. 2 (a)-(ii)**. Top frame illustrates the variation of the position in r, and the bottom that in θ. Note that the dashed line for r corresponds to the position of the periphery of the top/bottom rods ($r = 2.5$ mm). Particle number density is illustrated on the right of the top graph. The particle number is counted within a region of $\Delta r = 0.1$ mm. As aforementioned, the Poincaré section consists of three sets of pairs of the dense paths; in the vicinity of the free surface (as indicated as 'A' in **Fig. 2 (a)-(iii)**) and in the middle region of the liquid bridge (as indicated as 'B'). The positions in r for the particle to form PAS are divided into those two regions. In the distributions of the paths in θ, one finds three regions of the dense paths. When one pays attention to one of the regions, the region consists of further two area; coarser and denser ones. The former corresponds to the group 'A', and the latter to 'B'. This might be a sign to indicate that one of KAM tori, T_3^3, is a 'strong' attractor to keep the particles to form PAS as shown in **Fig. 2 (i)**.

We find that PAS would last more than about 50 fundamental periods of HTW especially under lower Ma concerned in the present study. Variation of attracting intensity against Ma is then examined. **Figure 4** (top) illustrates a typical example of the Poincaré section detected at z [mm] $= 0.81 \pm 0.09$ under Ma $= 5.2 \times 10^4$ (same as row (c) in **Fig. 2** but in the different experi-mental run). Note that the direction of HTW is counterclockwise in the laboratory frame in this case. Frames (a)-(c) indicate the
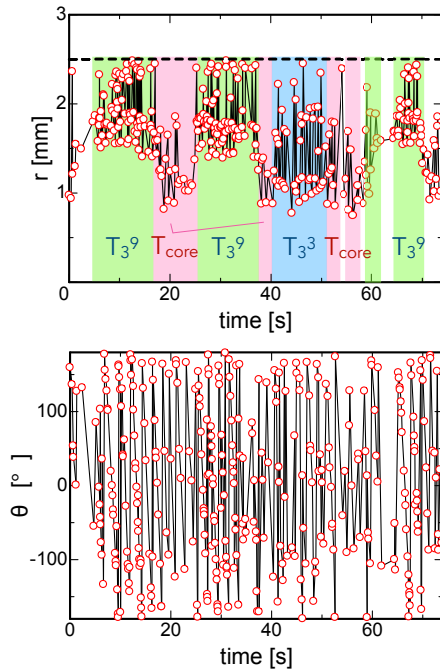

Fig. 5 Another example of temporal variations of (middle) r- and (bottom) θ-positions of a particle to migrate among structures on Poincaré section detected at z [mm] $= 0.79 \pm 0.09$ under Ma $= 5.2 \times 10^4$ (same as row (c) in Fig. 2 and Fig. 4 but in the different experimental run).

sections obtained in the same experimental run to track a single particle under the same condition but for different successive periods; frame (a) indicates the section obtained (a) $0 \le t$ [s] ≤ 6.1, (b) $6.1 \le t \le 33.4$, and (c) $33.4 \le t \le 73.2$. Frame (d) illustrates the whole and original Poincaré section obtained in a single experimental run for 73.2 s, that is, the sum of (a) to (c) corresponds to the original section. These successive sections imply that a single particle never stays to settle at a certain structure, but switches among specific structures. A single particle migrates from (a) the core first, then (b) stays for a while on a structure wrapping the core, and then finally (c) settles on PAS. As indicated by Kuhlmann et al.[35], each structure resembles to the KAM torus realized in the thermocapillary-driven convection in the half-zone liquid bridge. The structure known as the toroidal core resembles one of the tori T_{core}, whereas the structure wrapping the core resembles T_3^9. And PAS of $m = 3$ resembles T_3^3. It is noted that we confirm the corresponding torus T_3^9 by counting the number of wrapping around the core in the projected view in the frame of reference rotating with HTW. Such confirmation is available with the present experimental system; we monitor two different particles with different optical system, which enables us to check the spatial structure in a single experimental run without varying any conditions. In the middle and bottom frames of the figure, we indicate the corresponding temporal variations of r- and θ-positions of a particle on Poincaré section. In the variation of r-position, the corresponding KAM torus is indicated. Through this variations, one clearly see that the section (a) exhibits the paths of the particle on the core, that is, the particle is attracted by T_{core} first. Then, according to the section (b), the particles switches to the attractor T_3^9. But this torus does not keep attracting the particle; the particle migrates between the attractors T_3^9 and T_{core}. Finally, in this case, the particle is attracted to T_3^3 to keep forming PAS (the section (c)). Another exmaple of the particle migration among the structures is indicated in **Fig. 5**. In this case, it is found that the torus T_3^3 is not 'strong' attractor under this condition. That is, one observes that the particle switches the structure even from the torus T_3^3 to the others. This is the first demonstration of the particle migrations, and such migrations of a single particle among tori are observed more frequently under higher Ma.

Through the series of experiments, we might indicate that each structure becomes unstable to keep attracting particle under high Ma. It should be emphasized that, among the structures, the particle would not be able to stay in a long period especially at the core. Although we have not accumulated enough data in order to conduct a quantitative discussion, it is found that the period for the particle to stay at the core is rather short comparing to those for T_3^3 and T_3^9. Such feature agrees well with the prediction by Romanò & Kuhlmann[36]; the torus T_{core} in the high-Pr liquid bridge becomes weakly chaotic, and attracts the particles less than that in the fluids of lower-Pr of $\mathscr{O}(1)$ as indicated by
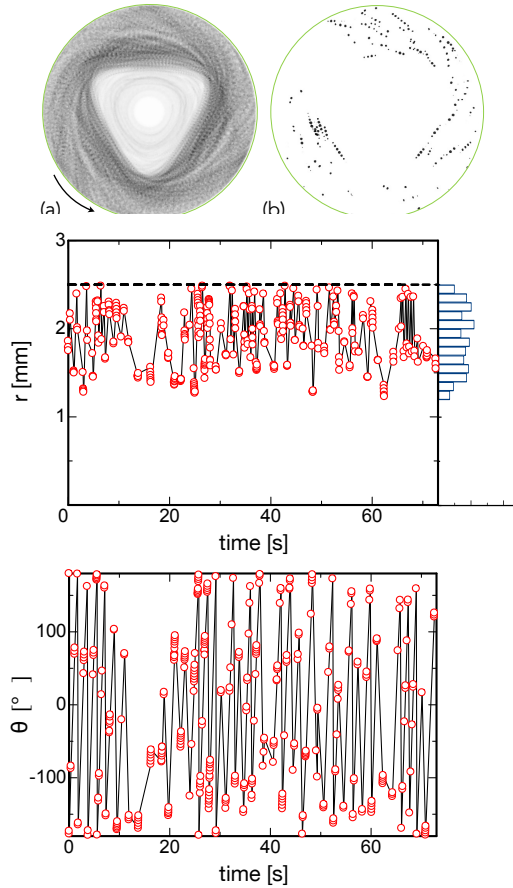
Fig. 6 (top) (a) Projected image (integrated for 7 s) and (b) Poincaré section (53 s) at midheight of liquid bridge observed through top rod in rotating frame of reference against fundamental frequency of hydrothermal wave (HTW) under $Ma = 2.1 \times 10^4$, and corresponding temporal variations of (middle) r- and (bottom) θ-positions of a particle on Poincaré section. Histogram on the right of top graph illustrates the particle number density measured with a constant interval $\Delta r = 0.1$ mm in the observation period. The direction of HTW is counter-clockwise in the laboratory frame in this case.

Mukin & Kuhlmann[33]. Futher researches should be required to examine the attractivity of each structure, and also examine the detail mechanism on the interaction between the particle and the structures.

In order to indicate unique characteristics of the particles' behavior to form PAS and the toroidal core, we illustrate the Poincaré section for a single partile suspended in the oscilla-tory regime under lower Ma without PAS. **Figure 6 (a)** illustrates the distribution of a number of particles suspended in the liquid bridge in the rotating frame of reference against the fundamental frequency of the oscillatory flow under $Ma = 2.1 \times 10^4$ ($\Delta T = 20$ K). The fluid exhibits a traveling-wave-type oscillatory convection as seen in those with PAS. The fundamental frequency f_0 under this condition is of 1.31 Hz, and the rotating direction of HTW

is counter-clockwise in the laboratory frame. This projected image is obtained by integrating for 7 s. While the high density regions of the paths are observed if PAS emerges in the liquid bridge (**Fig. 2**), the particles under the traveling flow without PAS distributes all over the liquid bridge excluding so-called depletion zone, and never exhibit any coherent structures. It has been known that the depletion zone where any particles never penetrate is formed[22,27,30,35] in the periodic oscillatory flows. The depletion zone has the same azimuthal wave number as HTW; one can see a triangle-shape depletion zone in this case. Frame (b) indicates the Poincaré section at z [mm] $= 0.75 \pm 0.09$ under the same condition as frame (a). This section represents the paths of a single particle accumulated for 53 s. Not only in the totally projected image but also in the Poincaré section, there exists an area in the middle, where the particle never penetrates. Middle and bottom frames indicate corresponding temporal variations of r- and θ-positions of a particle on Poincaré section, respectively. As also seen in the case of the flow field with PAS, the particle travels in an outer region in r, and does not travel into a region located in the central part of the liquid bridge. The minimum position of the particle in r, r_{min}, becomes larger than that for PAS r_{min}^{PAS} as indicated in **Figs. 3-5**. In the θ position, on the other hand, the paths never exhibit ordered distributions. This reflects that the region except the KAM tori (or regular region) consists of chaotic (or irregular) streamlines[36,40].

From these results, we indicate that the particles on PAS or toroidal core travel within limited region, where is similar to the KAM tori or regular regions when PAS is formed in the liquid bridge. We also indicate by monitoring the particle behaviors under lower Ma without forming PAS, the particle's motion is rather chaotic not to result in forming any coherent structures.

4. Concluding Remarks

We investigate behaviors of a single spherical particle in thermocapillary-driven flow in a so-called half-zone liquid bridge experimentally. Special attention is paid to those behaviors when the suspended particles form coherent structure known as the particle accumulation structure (PAS). We track the paths of the particle on PAS or in the toroidal core to illustrate the Poincaré section. In tracking the paths of the particle on PAS, we experimentally obtain three sets of pairs of the dense regions of paths inside the liquid bridge and in the vicinity of the free surface. In tracking the particle on the toroidal core, we obtained ring-like structure between the center and the free surface of the liquid bridge. Those distributions of the particle paths on PAS and the toroiral core quantitatively agree well with the structures of the regular regions or Kolmogolov-Arnold-Moser (KAM) tori predicted by Mukin and Kuhlmann[33].

It is found that the particle on PAS keeps traveling stably under low-enough Ma. Once the particle is trapped to that region, the particle is hardly detached from that area, and keeps staying to

form PAS. This implies the KAM torus of T_3^3 is a stable attractor in the flow field. As increasing the intensity of thermocapillary effect or Ma, it is found that the particle exhibits migrations among structures, and it is quite seldom for the particle to stay for a long period in that region. Among these, the region to form the core seems more unstable or less attractive to keep the particle. This is a sign to imply that the KAM tori of T_{core} and T_3^9 as well as T_3^3 are not stable attoractors anymore by increasing Ma if one employs the test fluids of $Pr = \mathcal{O}(10)$. It is quantitatively indicated that the region of the core, resembling T_{core}, becomes less attractive comparing to the other two. This result supports the prediction by the numerical simulation by Romanò & Kuhlmann [36], in which they indicated that the core becomes rather chaotic in the case of $Pr = 28$. Such trend is different from the lower Pr case as indicated [33].

We also indicate the Poincaré section of a single particle under lower Ma when the suspended particles never exhibit PAS but show a particle depletion zone in the traveling flow regime. There exist no dense regions of the paths at all; the paths distribute all over the section except the depletion zone. It is indicated that no KAM tori with a sharp and narrow structure are formed in the convective field under Ma beneath the threshold to form PAS.

Acknowledgments

References

1) H. Kawamura, I. Ueno and T. Ishikawa: Advances in Space Research, **29** (2002) 611.

2) M. K. Smith and S. H. Davis: Journal of Fluid Mechanics, **132** (1983) 119.

3) J.-J. Xu and S. H. Davis: Journal of Fluid Mechanics, **161** (1985) 1.

4) T. Yano, K. Nishino, H. Kawamura, I. Ueno, S. Matsumoto, M. Ohnishi and M. Sakurai: Journal of Physics: Conference Series, **327** (2011) 012029.

5) H. Kawamura, K. Nishino, S. Matsumoto and I. Ueno: Journal of Heat Transfer, **134** (2012) 031005.

6) T. Yano, K. Nishino, H. Kawamura, I. Ueno, S. Matsumoto, M. Ohnishi and M. Sakurai: Experiments in Fluids, **53** (2012) 9.

7) K. Nishino, T. Yano, H. Kawamura, S. Matsumoto, I. Ueno and M. K. Ermakov: Journal of Crystal Growth, **420** (2015) 57.

8) T. Yano, K. Nishino, H. Kawamura, I. Ueno and S. Matsumoto: Physics of Fluids, **27** (2015) 024108.

9) F. Sato, I. Ueno, H. Kawamura, K. Nishino, S. Matsumoto, M. Ohnishi and M. Sakurai: Microgravity Science and Technology, **25** (2013)(1) 43.

10) T. Matsugase, I. Ueno, K. Nishino, M. Ohnishi, M. Sakurai, S. Matsumoto and H. Kawamura: International Journal of Heat and Mass Transfer, **89** (2015) 903.

11) T. Watanabe, T. Takakusagi, I. Ueno, H. Kawamura, K. Nishino, M. Ohnishi, M. Sakurai and S. Matsumoto: International Journal of Heat and Mass Transfer, **123** (2018) 945.

12) T. Yano, K. Nishino, I. Ueno, S. Matsumoto and Y. Kamotani: Physics of Fluids, **29** (2017) 044105.

13) T. Yano, K. Nishino, S. Matsumoto, I. Ueno, A. Komiya, Y. Kamotani and N. Imaishi: Microgravity Science and Technology, **30** (2018) 599.

14) T. Yano, K. Nishino, S. Matsumoto, I. Ueno, A. Komiya, Y. Kamotani and N. Imaishi: International Journal of Microgravity Science and Application, **35** (2018) 350102.

15) D. Schwabe, P. Hintz and S. Frank: Microgravity Science and Technology, **9** (1996) 163.

16) H. C. Kuhlmann, M. Lappa, D. E. Melnikov, R. Mukin, F. H. Muldoon, D. O. Pushkin, V. M. Shevtsova and I. Ueno: Fluid Dynamics and Materials Processing, **10** (2014)(1) 1.

17) V. Shevtsova, Y. Gaponenko, H. C. Kuhlmann, M. Lappa, M. Lukasser, S. Matsumoto, A. Mialdun, J.-M. Montanero, K. Nishino and I. UENO: Fluid Dynamics and Materials Processing, **10** (2014)(2) 197.

18) M. Wanschura, V. M. Shevtsova, H. C. Kuhlmann and H. J. Rath: Physics of Fluids, **7** (1995)(5) 912.

19) K. Fujimura: Journal of Physical Society of Japan, **82** (2013) 074401.

20) S. Frank and D. Schwabe: Experiments in Fluids, **23** (1997)(3) 234.

21) J. Leypoldt, H. C. Kuhlmann and H. J. Rath: Journal of Fluid Mechanics, **414** (2000) 285.

22) I. Ueno, S. Tanaka and H. Kawamura: Physics of Fluids, **15** (2003)(2) 408.

23) S. Tanaka, H. Kawamura, I. Ueno and D. Schwabe: Physics of Fluids, **18** (2006) 067103.

24) D. Schwabe, A. I. Mizev, M. Udhayasankar and S. Tanaka: Physics of Fluids, **19** (2007) 072102.

25) Y. Abe, I. Ueno and H. Kawamura: Dynamic particle accumulation structure due to thermocapillary effect in noncylindrical half-zone liquid bridge, *Ann. N. Y. Acad. Sci.*, vol. 1161: New York Academy of Sciences, 2009, 240–245.

26) Y. Niigaki and I. Ueno: Trans. JSASS (Japan Soc. for Aeronautical and Space Sciences, Aerospace Technology), **10** (2012) Ph33.

27) A. Toyama, M. Gotoda, T. Kaneko and I. Ueno: Microgravity Science and Technology, **29** (2017)(4) 263.

28) D. O. Pushkin, D. E. Melnikov and V. M. Shevtsova: Physical Review Letters, **106** (2011) 234501.

29) E. Hofmann and H. C. Kuhlmann: Physics of Fluids, **23** (2011)(7) 072106.

30) F. H. Muldoon and H. C. Kuhlmann: Physica D: Nonlinear Phenomena, **253** (2013)(15) 40.

31) F. Romanò, H. C. Kuhlmann, M. Ishimura and I. Ueno: Physics of Fluids, **29** (2017) 093303.

32) H. C. Kuhlmann and F. H. Muldoon: Physical Review E, **85** (2012) 046310.

33) R. V. Mukin and H. C. Kuhlmann: Physical Review E, **88** (2013) 053016.

34) T. Ogasawara, K. Motegi, T. Hori and I. Ueno: Mechanical Engineering Letters, **5** (2019) accepted (1st Mar. 2019).

35) H. C. Kuhlmann, R. V. Mukin, T. Sano and I. Ueno: Fluid Dynamics

Research, **46** (2014) 041421.

36) F. Romanò and H. C. Kuhlmann: Physical Review Fluids, **3** (2018) 094302.

37) M. Gotoda, T. Sano, T. Kaneko and I. Ueno: European Physical Journal Special Topics, **224** (2015) 299.

38) Shin-Etsu Chemical Company Limited: Technical Data: Silicone fluid KF96 Performance Test Results: Tech. rep., Shin-Etsu Chemical Co., Ltd. (2014).

39) M. Gotoda, D. E. Melnikov, I. Ueno and V. Shevtsova: Chaos, **26** (2016) 073106.

40) F. H. Muldoon and H. C. Kuhlmann: International Journal of Multiphase Flow, **59** (2014) 145.